Turbulence, Heat and Mass Transfer 6
K. Hanjalić, Y. Nagano and S. Jakirlić (Editors)

Active control of swirling coaxial jet mixing with manipulation of large-scale vortical structures

Y. Saiki, Y. Suzuki and N. Kasagi
Department of Mechanical Engineering, The University of Tokyo, Hongo 7-3-1, Bunkyo-ku, Tokyo 113-8656, Japan
saiki@thtlab.t.u-tokyo.ac.jp, ysuzuki@thtlab.t.u-tokyo.ac.jp, kasagi@thtlab.t.u-tokyo.ac.jp

Abstract – Large-scale vortical structures and associated mixing in methane/air swirling coaxial jets are actively controlled by manipulating the outer shear layer of the outer swirling coaxial jet with miniature flap actuators. In order to investigate the control mechanism, stereoscopic PIV and PLIF techniques are employed. As a result, intense vortex rings are produced in the outer shear layer in phase with the periodic flap motion regardless of the swirl rate examined. Vortical structures in the inner shear layer, however, are strongly dependent on the swirl rate. This is due to the fact that the central methane jet is accelerated by the swirl in the outer jet. At a relatively low swirl rate, the inner vortices are shed continuously and the methane jet is pinched off. This particular mode promotes the mixing of methane and air, so that the flammable mixture can be formed in an earlier stage of jet flow development.

1. Introduction

Small-scale distributed generation (DG) systems are expected to play a major role in the future society with lower environmental impacts. Micro gas turbines (MGT) of 1-100 kW power output are considered as a core technology in DG systems. However, downsizing of such gas turbines may cause various problems. For instance, small combustors for MGT are operated at a wide range of partial load, where it is difficult to keep with flame stability, high combustion efficiency and low nitrogen oxides emission. Swirling jet is often employed in gas turbine combustors, as swirl provides reliable flame anchoring near the burner outlet. Since the performance of passive devices such as swirler is deteriorated under off-design conditions, active combustion control should be introduced to have an ideal flame under variable load conditions.

For no-swirling jets, it is well known that perturbations in the jet shear layers are amplified through shear layer and/or column mode instabilities and result in large-scale vortical structures. Since the development of such vortices is extremely sensitive to the shear layer excitation, bulk forcing with acoustic speakers was often employed in single and coaxial jets to alter the flow structures and enhance turbulent mixing [1-3]. Also in swirling jets and flames, introducing disturbances into the shear layer can be a key tool to control the large-scale structures. The effects of forcing on single swirling jets at various frequencies, amplitudes and azimuthal modes were investigated. Panda and MacLaughlin [4] reported the influence of swirl on the amplification of the inherent instabilities in a swirling air jet. They found that axisymmetric or azimuthal forcing intensified the instabilities and successfully lead to regular organized structures. At higher swirling rate condition, however, Gallaire et al. [5] shown that the receptivity of the jet was very poor and the structure of vortex breakdown was unaffected by low amplitude forcing. In contrast, Alekseenko et al. [6] examined the detailed flow structure of a swirling jet forced axisymmetrically at various amplitudes through a

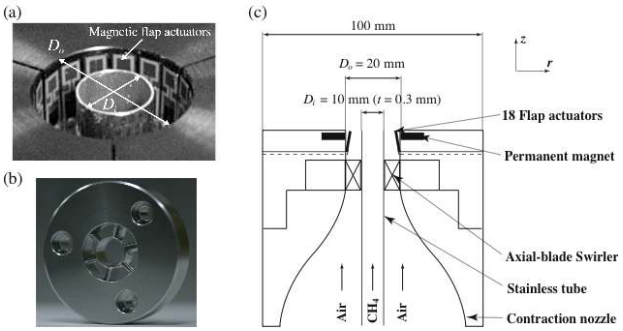

Fig. 1 Coaxial jet nozzle: (a) flap actuators equipped inside the nozzle, (b) axial-blade swirler, and (c) cross section view.

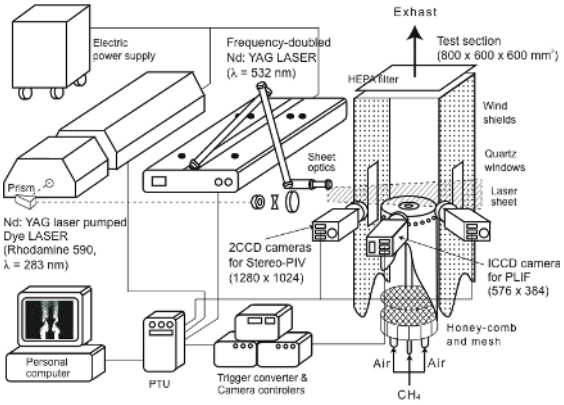

Fig. 2 Schematic of stereo-PIV/PLIF measurement setup.

stereoscopic PIV technique. They demonstrated that combined high swirl and external forcing can be efficient for jet mixing enhancement.

Recently, advanced control schemes of turbulent and thermal phenomena have been intensively studied. In particular, development of micro electro-mechanical systems (MEMS) has made it possible to fabricate small enough device such as micro actuators for flow control. For instance, Kurimoto et al. [7] applied micro flap actuators [8] to an axisymmetric coaxial nozzle and excited the initial jet shear layer. It was found that vortex rings were produced perfectly in phase with the flap motion and mixing can be flexibly controlled by changing the flapping frequency.

The objectives of the present study are to manipulate large-scale vortical structures and control mixing in a methane/air swirling coaxial jet, which is widely used in combustion furnaces. As the flow control device, the micro flap actuators are employed. Unlike the conventional bulk-forcing scheme, the flapping motion can introduce disturbances into the initial jet shear layer directly, and the control frequency can be modified according to the flow conditions. Therefore, there is a possibility that the vortical structures and associated mixing can be manipulated more flexibly with a smaller power input. In this work, we explore the effect of the swirl intensity and the flapping frequency on the control results through stereoscopic particle image velocimetry (stereo-PIV) and planar laser-induced fluorescence (PLIF) techniques.

2. Experimental setup

2.1. Flow facility

Figure 1 shows a swirling coaxial jet nozzle equipped with miniature magnetic flap actuators. A swirling air jet is supplied into a test section (800 x 600 x 600 mm^3) through an annular nozzle (inner diameter D_i = 10 mm, outer diameter D_o = 20 mm). Swirl in the annular jet is generated by means of six curved guide vanes attached to the outer surface of a cylindrical center body and the vane angle is changed to be 30° and 45° at the exit. The degree of swirl can be characterized by the swirl number, S. The swirl number is calculated from the mean streamwise and tangential components [9] at the nozzle exit measured through a stereo-PIV technique. In order to investigate the effect of the swirl intensity on the mixing process, S is set to be 0.2 and 0.4 in this study. A central methane jet is supplied from a long stainless tube (outer diameter D_i = 10 mm, thickness t = 0.3 mm), in which fully developed laminar flow is established. The bulk mean velocities of central and annular jets are $U_{m,\,i}$ = 0.38 m/s and $U_{m,\,o}$

= 1.8 m/s, respectively. The Reynolds number of the annular jet, $U_{m,\,o}D_o/\nu_o$, and the momentum flux ratio, $\rho_0 U_{m,\,o}^2/\rho_1 U_{m,\,i}^2$, are respectively 2.4 x 10^3 and 42, which are equivalent to a 1.0 kW jet flame.

Eighteen flap actuators are installed on the inner surface of the annular nozzle, so that the induced velocity is introduced into the outer swirling jet shear layer. The number of flaps is equal to the integral multiple of that of the swirler blades. Thus, the control inputs are given to each of the jet flows divided by the swirler. In this study, the trigger signal for flapping motion is a saw-wave form. After reaching the maximum displacement of 0.3 mm above the nozzle wall surface, the flaps come down to their original position. Large negative and positive radial velocities (~ $0.2U_{m,\,o}$) are induced in the outer shear layer by the quick snapping motion. In the case of a no-swirling coaxial jet, they result in vortex ring formation within a short distance from the nozzle [10]. The power consumption per flaps is negligibly smaller than the thermal power of the assumed flame. In a series of experiments, the motions of flaps are all synchronized. The Strouhal number St_a (= $f_a D_o/U_{m,\,o}$) is defined with flapping frequency f_a, and St_a is changed from 0.3 to 1.6.

2.2. Measurement setup

A schematic of the measurement setup is shown in Fig. 2. Stereo-PIV is employed for two-dimensional three velocity components measurement. The central and annular jets are seeded with silica particles (d_p = 1.2 μm, ρ_p = 215 kg/m^3). The particle relaxation time τ_p is 0.95 μs [11], which is much smaller than the Kolmogorov time scale τ_s ~ 221 μs estimated by $D_o^2 \mathrm{Re}^{-3/2}/\nu_o$, so that we can assume the particle traceability to the flow. A double-pulsed Nd: YAG laser (THALES, SAGA PIV 20) is employed as a light source and the laser sheet of ~ 1.5 mm thickness is introduced into the test section. Particle images are captured by two flame-straddling CCD cameras (Lavision, Flowmaster 3S), which are arranged in a scheimpflug condition. The angle between the CCD cameras is 90° in order to maximize the accuracy in the out-of-plane component measurement [12]. Commercial software (Lavision, Davis 7.2) is used to calculate the particle displacement in an interrogation area with a cross-correlation technique. In order to transform the recorded images into the object plane coordinate system, the third order polynomial imaging function, which provides more accurate calibration results than imaging functions of lower order, is selected. The size of interrogation area is 32 x 32 pixels^2, which corresponds to 1.6 x 1.6 mm^2. An overlap of 50% of the interrogation area is used in all cross-correlation. The time interval of the laser pulses is set to be 70 μs in order to minimize the influence of the velocity gradient in the shear layer [13]. The uncertainty intervals estimated at 95% coverage for the instantaneous velocities u (= 1.8 m/s) and w (= 1.0 m/s) are 0.12 m/s and 0.14 m/s, respectively.

Mixture fraction of methane is measured by acetone-PLIF. The central methane jet is seeded with acetone vapor. For the measurement of acetone fluorescence, UV laser pulse of 283.0 nm is generated with a frequency-doubled dye laser (Lambda Physik, SCANmate2C), which is pumped by a doubled Nd: YAG laser. The laser beam is formed into a laser sheet of constant height (60 mm) and thickness (0.5 mm) by using cylindrical lenses, then the laser sheet is introduced into the test section. The fluorescence signal is detected with an image intensified CCD camera (Lavision, Flamestar2), and spatial resolution is 0.4 x 0.4 mm^2. The fluorescence intensity at each pixel is converted to the instantaneous volumetric mixture fraction c. Taking into account the shot noise in the weak light detection, the uncertainty intervals at 95% is 0.015 for c = 0.1.

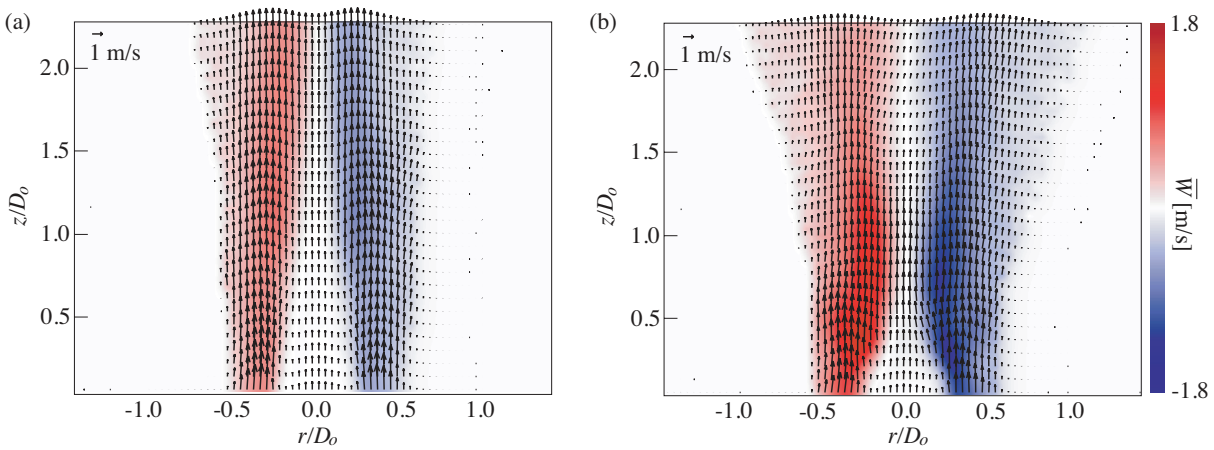

Fig. 3 Mean velocity field of uncontrolled swirling coaxial jets. Vectors denote streamwise and radial components, and gradation tangential component: (a) S = 0.2, and (b) S = 0.4.

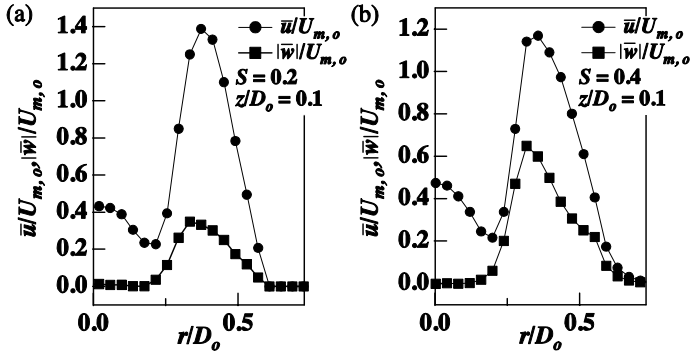

Fig. 4 Radial distribution of mean streamwise and tangential velocities at z/D_o = 0.1.

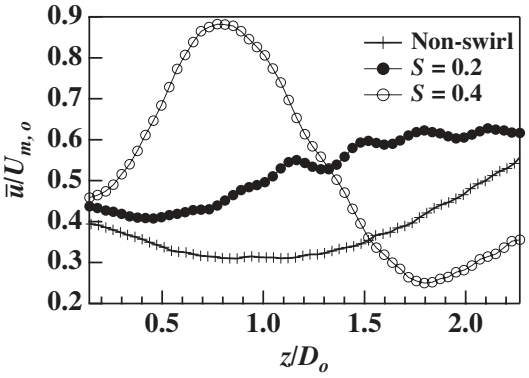

Fig. 5 Axial distribution of mean streamwise velocity along the center axis for uncontrolled jet.

3. Results

3.1. Uncontrolled swirling jet

Figure 3 shows the mean velocity field of uncontrolled swirling coaxial jet with S = 0.2 and 0.4 in the central longitudinal plane, while corresponding radial distributions of mean steamwise and tangential velocities at the nozzle exit (z/D_o = 0.1) are shown in Fig. 4. The maximum tangential velocities at the nozzle exit with S = 0.2 and 0.4 are 0.7 m/s (~0.39$U_{m,o}$) and 1.1 m/s (~0.61 $U_{m,o}$), respectively. Note that the maximum streamwise velocity of S = 0.4 is slightly lower than that of S = 0.2. This is due to the fact that the jet flow is separated at the swirler vanes, and thus azimuthal distributions of the streamwise velocity become inhomogeneous. In the present conditions, a vortex breakdown does not appear, and a central recirculation zone is not formed for relatively low swirl numbers [14]. The development of the outer swirling jet shear layer becomes earlier as the swirl rate is increased. In addition, it is found that the central methane jet is accelerated rapidly at z/D_o < 0.8, especially when S = 0.4.

The axial distributions of mean streamwise velocity along the center axis for non-swirling and swirling jets are shown in Fig. 5. Since a negative pressure gradient along the center axis

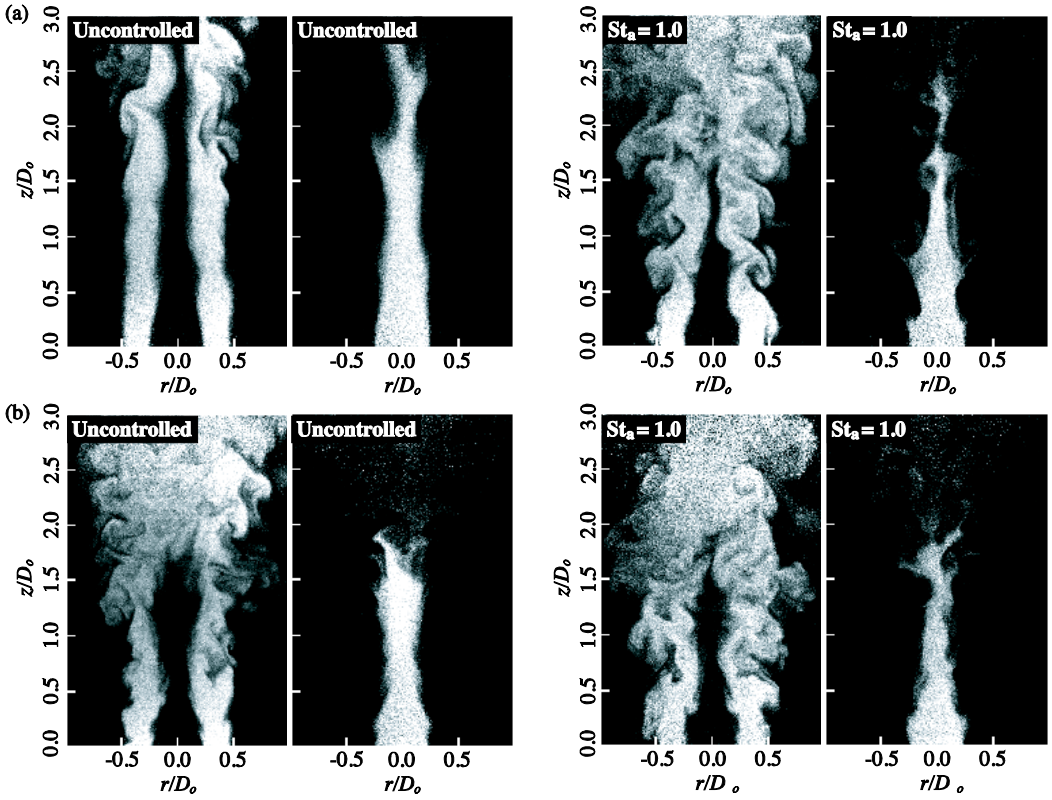

Fig. 6 Instantaneous visualization images of uncontrolled and controlled jets with St_a = 1.0: (a) S = 0.2, and (b) S = 0.4.

is generated by the swirl, the central velocity in the nozzle-near field is accelerated significantly with increase of swirl intensity. This phenomenon is qualitatively consistent with the velocity and pressure measurement results by Champagne and Kromat [15].

3.2. Controlled swirling jet

3.2.1. Influence of swirl intensity on the control effect

Instantaneous PLIF images of the uncontrolled and controlled swirling jets with St_a = 1.0 for S = 0.2 are compared in Fig. 6a, where acetone vapor is separately seeded in the central or annular fluid. The inner and outer shear layers in the uncontrolled jet start to roll up into large-scale vortex rings at z/D_o = 1.5 ~ 2.0 through the column-mode instability. On the other hand, in the controlled jet, the both shear layers are forced to roll up quickly into large-scale axisymmetric vortices. The produced inner vortices pinch off the central jet, and this promotes the mixing of methane and air. It is found that these vortices are shed perfectly in phase with the flap motion under various flapping St_a conditions tested.

Figure 6b shows images at S = 0.4. In comparison with S = 0.2, the central potential core length of the uncontrolled jet is reduced due to the prompted growth of swirling jet shear layer. In the controlled jet, as is the case with S = 0.2, large-scale vortices are shed in the outer shear layer, but, there is no significant change in the inner shear layer.

In order to detect the vortices, the second invariant of the deformation tensor is used in the present study.

$$Q = \frac{\partial u_i}{\partial x_j} \cdot \frac{\partial u_j}{\partial x_i} \tag{1}$$

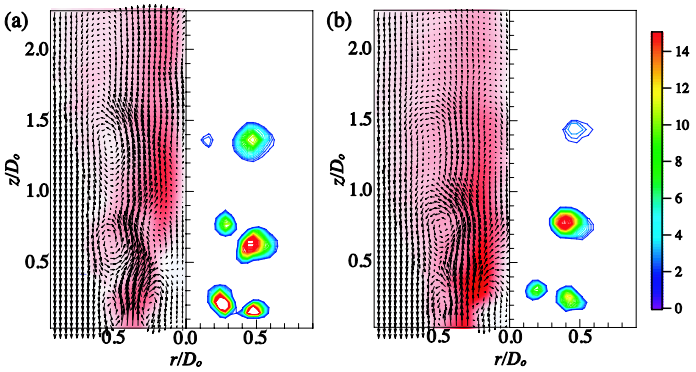

Fig. 7 Phase-averaged velocity fields and contours of Q (< 0) for controlled jets at St_a = 1.0: (a) S = 0.2, and (b) S = 0.4.

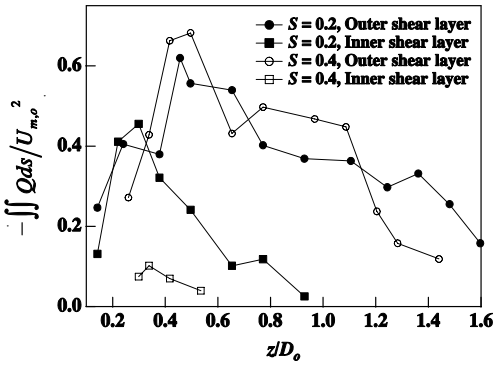

Fig. 8 Streamwise variation of vortex strength of controlled jets with St_a = 1.0 at S = 0.2 and 0.4.

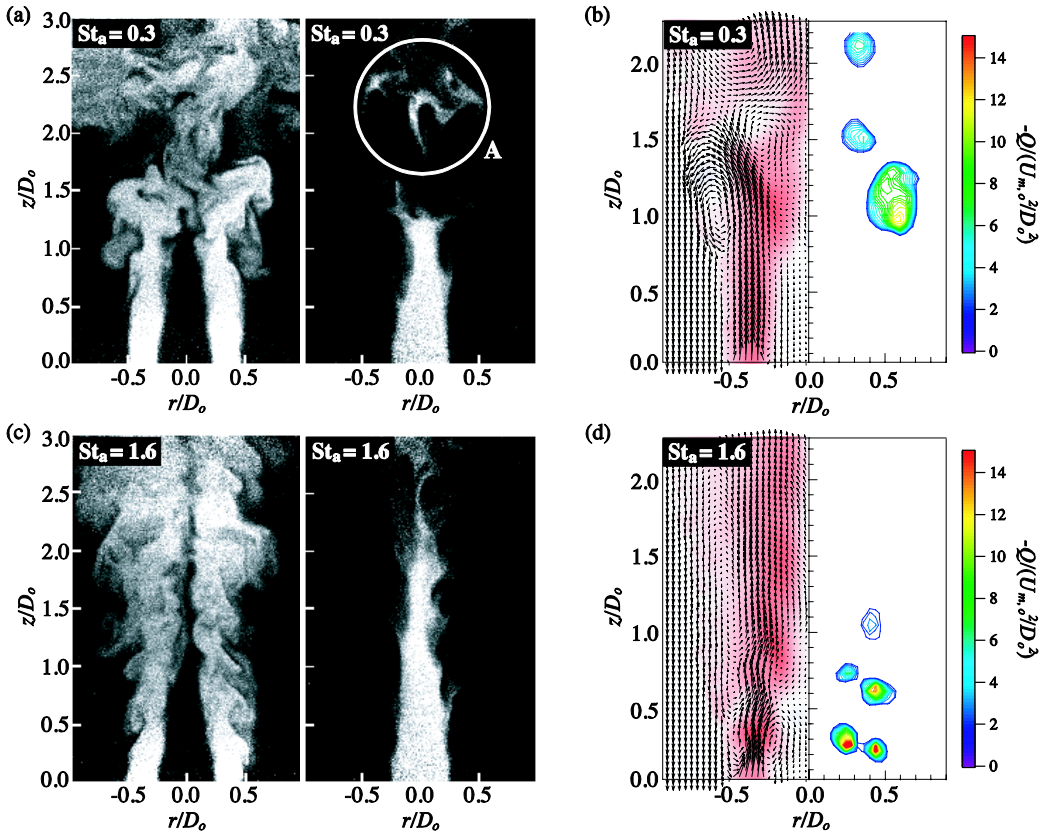

Fig. 9 Instantaneous visualization images and phase-averaged velocity fields and contours of Q (< 0) for controlled swirling jets with S = 0.2: (a, b) St_a = 0.3, and (c, d) St_a = 1.6.

Figure 7 represents phase-averaged velocity fields ($\phi = 0.6\pi$) and contours of the second invariant of deformation tensor Q (< 0) in controlled jets at St_a = 1.0 with S = 0.2 and 0.4. Note that the convection velocity of the vortex ring ($U_c = 0.5U_{m,o}$) is subtracted from the velocity field in order to visualize the vortical motions [16]. In the outer swirling jet shear layers (r/D_o = ~0.5), vortex rings formed continuously by the flaps are clearly observed regardless of the swirl number. On the other hand, vortex shedding in the inner shear layer (r/D_o = ~0.25) is strongly dependent on the swirl rate. Figure 8 shows streamwise variation of the vortex strength in the inner and outer jet shear layers of the controlled jets. In this study,

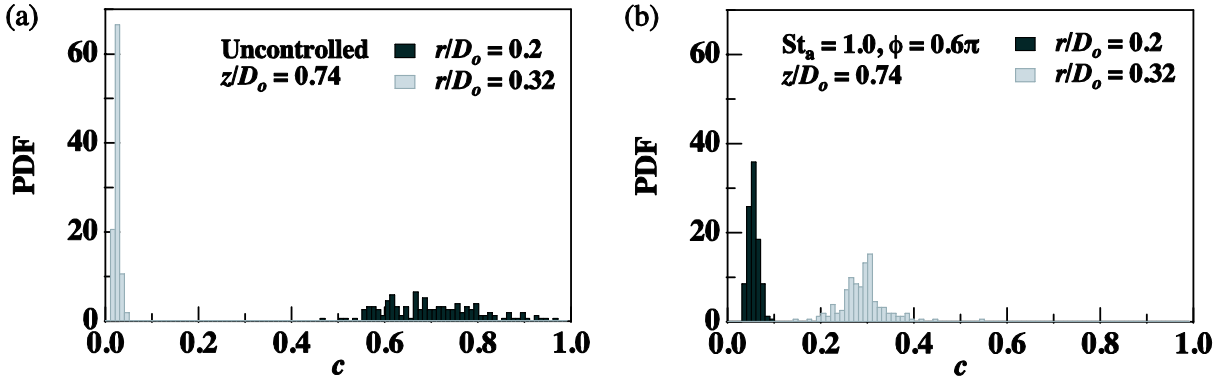

Fig. 10 PDF of mixture fraction in uncontrolled and controlled swirling jets with S = 0.2 at z/D_o = 0.74 and r/D_o = 0.2, 0.32: (a) uncontrolled, and (b) St_a = 1.0.

the integration of Q, where Q is lower than 5 percent of a local minimum, is taken as the vortex strength. It is clearly seen that the strength of the inner vortices is weaker than that of the outer vortices at both swirl rate conditions. Especially in S = 0.4, intense vortices can not be formed. Kurimoto et al. [1] showed that the inner vortices, which have the same strength as the outer ones, can be produced by the flap in no-swirling coaxial jet at the same Reynolds number (= 2400) and momentum flux ratio (= 42) conditions. The weakening of the inner vortices is mainly due to a fact that the central jet is accelerated by the swirl in annular jet as previously mentioned, and thus momentum flux ratio, $\rho_o U_o^2 / \rho_i U_i^2$, at the nozzle near-field is significantly reduced. Therefore, it is important for the mixing control in swirling coaxial jets to set initial momentum flux ratio, $\rho_o U_{m,o}^2 / \rho_i U_{m,i}^2$, relatively low by adjusting the nozzle diameter ratio, D_o/D_i.

3.2.2. Effect of flapping frequency

Hereafter, the effect of flapping St_a on the flow structure and associated mixing in the coaxial swirling jet is discussed. The swirl intensity is fixed at S = 0.2, where relatively intensive vortices can be shed in the inner shear layer.

Figure 9 shows instantaneous images, and corresponding phase-averaged velocity fields and contours of Q (< 0) with St_a = 0.3 and 1.6. When St_a = 0.3, larger vortices are produced. Since the interval of the vortex shedding is about three times larger than that of St_a = 1.0, the vortex convects further downstream before the vortex shedding in the next control period. As a result, the vortices pinch off the central jet intermittently and the inner fluid is divided into streamwise direction (A in Fig. 9a).

On the other hand, when St_a = 1.7, relatively small-scale vortices are shed continuously, so that the deformation of the swirling jet shear layer is small. Therefore, the central fluid is not significantly transported outward and the local mixing is performed only near the inner shear layer.

In order to investigate the mixing behavior quantitatively, the mixture fraction is calculated from acetone fluorescence intensity. Figure 10 shows probability density function (PDF) of mixture fraction in the uncontrolled and controlled jets at z/D_o = 0.74 and r/D_o = 0.2, 0.32, where the inner vortex ring produced by the flap is located as shown in Fig. 7a. Note that PDF of the controlled jet is calculated from 150 phase-locked PLIF images at $\phi = 0.6\pi$. In the uncontrolled jet, fuel-rich mixture (c = ~0.7) with large fluctuation exists at r/D_o = 0.2, whilst PDF has a peak value at $c \sim 0$ and r/D_o = 0.32. On the other hand, in the controlled jet, fuel-lean mixture (c = ~0.05) with relatively small fluctuation is formed at r/D_o = 0.2 and the

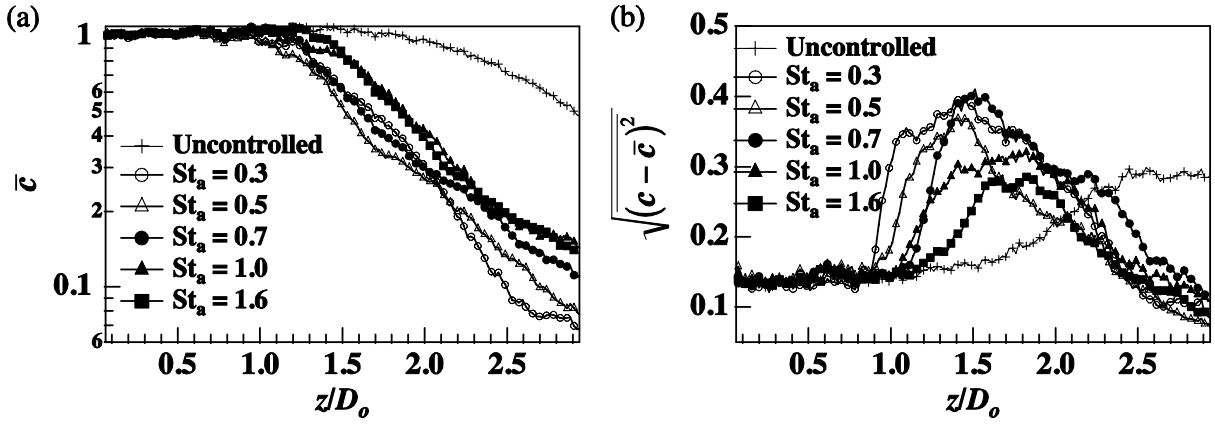

Fig. 11 Streamwise distribution of mixture fraction in uncontrolled and controlled swirling jets (S = 0.2) at center axis: (a) mean, and (b) rms fluctuation.

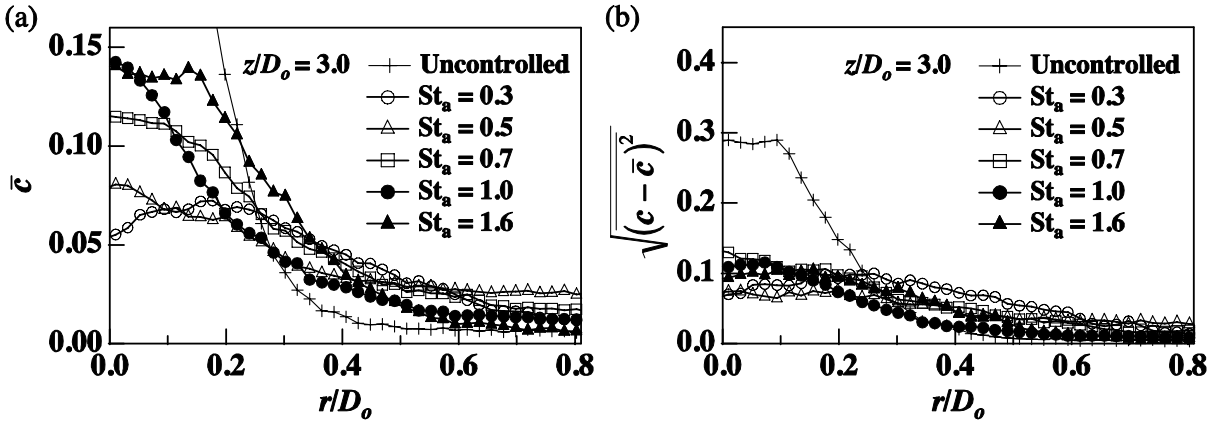

Fig. 12 Radial distribution of mixture fraction in uncontrolled and controlled swirling jets (S = 0.2) at z/D_o = 3.0: (a) mean, and (b) rms fluctuation.

peak value position of PDF at r/D_o = 0.32 is shifted to c ~ 0.3. This indicates that the outer air flow is brought toward the jet axis and also the inner methane is transported in the radial direction by the vortical motion. Therefore, the inner vortex ring plays an important role in promoting transportation and mixing of inner and outer fluids.

Figure 11 shows the distributions of mean and rms fluctuation of mixture fraction along the jet axis in the uncontrolled and controlled jets with different flapping frequencies, St_a = 0.3-1.6. The statistical values are calculated from 500 instantaneous images captured with $\Delta\phi = \pi/20$. In the uncontrolled jet, the inner potential core lemgth, where $\bar{c}$ is almost unity, is $1.5D_o$, and $\bar{c}$ is gradually decreased downstream due to the naturally occurring vortices. With respect to the rms fluctuation, $\sqrt{\overline{(c-\bar{c})^2}}$, it is gradually increased from the inner potential core end (z/D_o = ~ 1.5) and reaches the maximum value of 0.3 at $z/D_o \fallingdotseq 2.5$. Note that $\sqrt{\overline{(c-\bar{c})^2}}$ is not zero within the potential core due to the shot noise.

On the other hand, in the controlled jets, the inner core length is shortened to $0.9\sim1.2D_o$ and $\bar{c}$ is decreased rapidly for the inner vortices produced by the flap. In addition, $\sqrt{\overline{(c-\bar{c})^2}}$ is significantly increased from the inner core end and the position of the maximum value is shifted to upstream compared to that of the uncontrolled jet. In particular, when St_a is smaller than unity, the maximum value becomes enormous and reaches about 0.4 at $z/D_o \fallingdotseq 1.5$. This

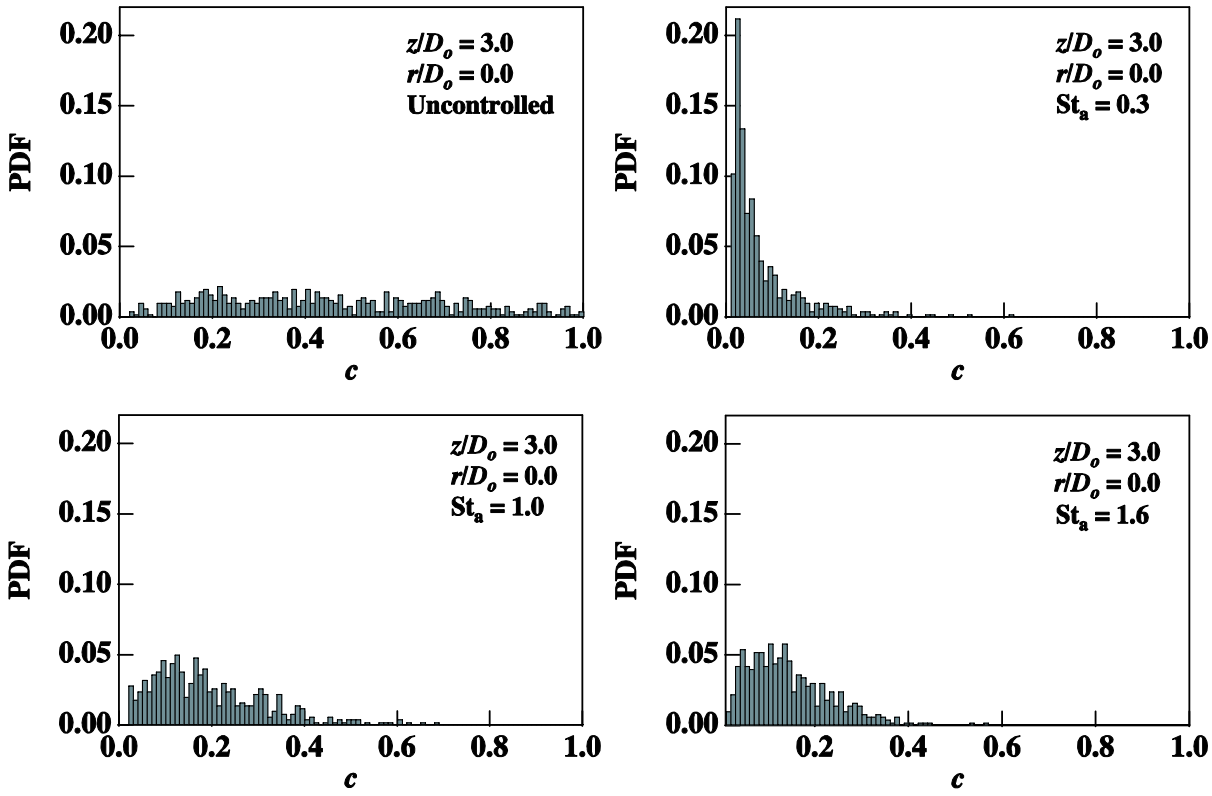

Fig. 13 PDF of mixture fraction in uncontrolled and controlled swirling jets (S = 0.2) at z/D_o = 3.0 and r/D_o = 0.0: (a) uncontrolled, (b) St_a = 0.3, (c) St_a = 1.0, and (d) St_a = 1.6.

implies that the vortex shedding is discontinuous due to the low St_a conditions as shown in Fig. 9 and thus the transport of inner and outer fluids becomes intermittent.

Figure 12 shows radial distributions of mean and rms fluctuation of mixture fraction at z/D_o = 3.0. It is found that the radial transport range can be controlled by changing St_a. This is because that the diameter of the vortex rings becomes smaller as St_a is increased as previously mentioned. When $St_a << 1.0$, methane is significantly transported to the radial direction by the vortex rings of large diameter. On the other hand, when $St_a \geqq 1.0$, the mixing is locally enhanced near the inner shear layer by the vortex rings of relatively small diameter. It is known that the flammable limit for methane/air mixture is $0.05 \leqq c \leqq 0.15$. Therefore, the flammable mixture can be formed in an early stage of the jet flow development by the present control method.

As shown in Fig. 12b, the fluctuation values of mixture fraction is suppressed in all controlled jets compared with that of the uncontrolled jet.

In order to investigate the fluctuation of mixture fraction in detail, the PDF of instantaneous mixture fraction in the uncontrolled and controlled jets with St_a = 0.3, 1.0 and 1.6 is shown in Fig. 13. The PDF of the uncontrolled jet has no peak values and the associated fluctuation is enormous. When St_a = 0.3, the PDF has a peak value at $c \sim 0$. It means that the vortex shedding is discontinuous due to low St_a, and thus the passing of mixture is intermittent. On the other hand, when St_a = 1.0 and 1.6, the PDF has a peak value at $c \sim 0.15$ for the periodic shedding of the vortex ring.

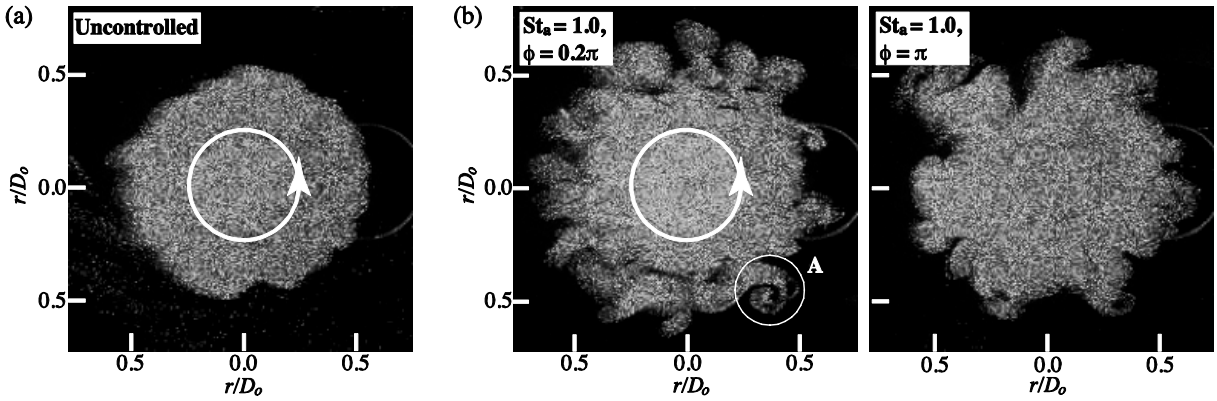

Fig. 14 Instantaneous cross-sectional images of uncontrolled and controlled swirling jet with St_a = 1.0 (S = 0.2) at z/D_o = 0.5: (a) uncontrolled, and (b) St_a = 1.0.

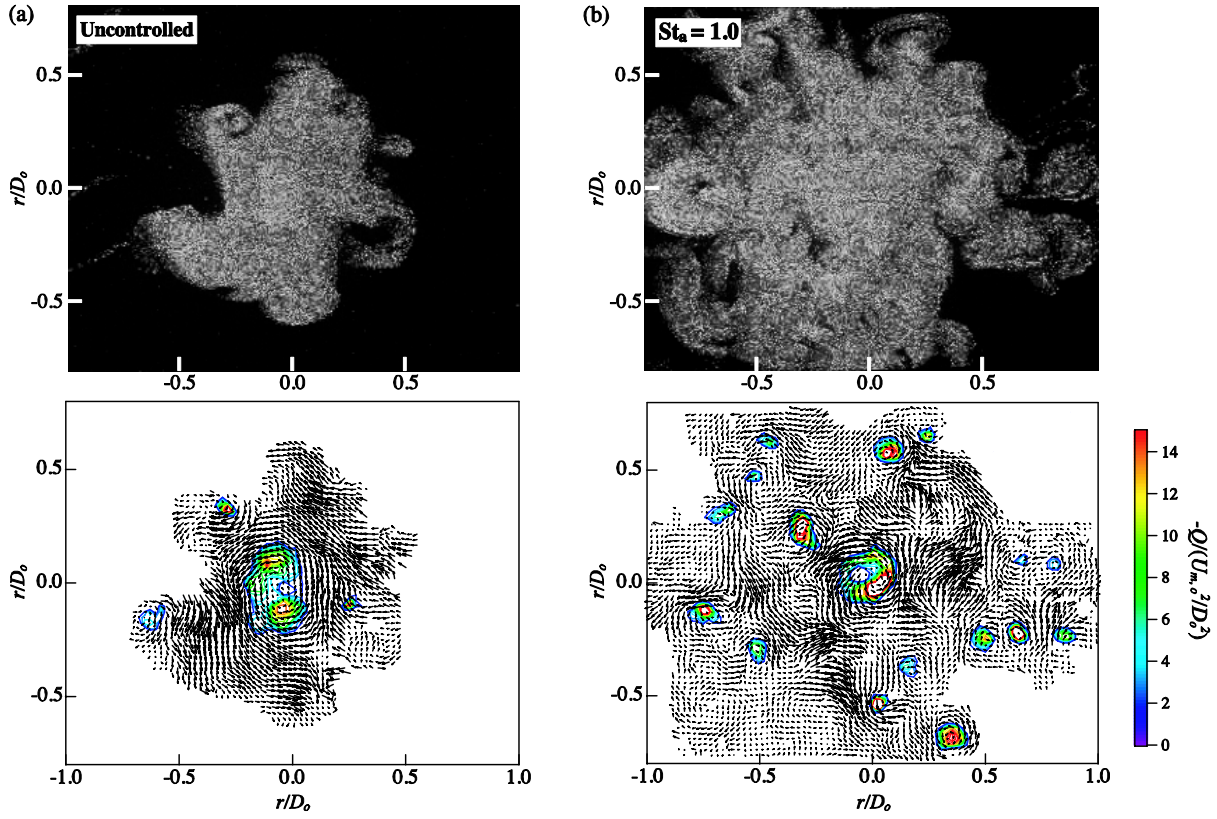

Fig. 15 Instantaneous cross-sectional images and instantaneous velocity fields with superimposed contour of Q (< 0) for uncontrolled and controlled swirling jet with St_a = 1.0 (S = 0.2) at z/D_o = 2.0: (a) uncontrolled, and (b) St_a = 1.0.

In summary, when $St_a \geqq 1.0$, the vortex shedding becomes continuous, so that the transport and mixing of methane/air fluids are promoted. Therefore, the flammable mixture with relative small fluctuation can be formed in an earlier stage compared to the uncontrolled jet. In addition, the radial transportation range can be controlled by changing St_a.

3.2.3. Cross-sectional flow structure

Finally, cross-sectional flow structures of the swirling jet with S = 0.2 are investigated. Figure 14 shows instantaneous cross-sectional PIV images of the uncontrolled and controlled jet with St_a = 1.0 at z/D_o = 0.5. The images are captured by the Stereo-PIV camera with the scheimpflug configuration and reconstructed into the object plane coordinate system through the imaging function. The imposed rotation is anti-clockwise as shown in the figure. In the uncontrolled jet, the jet shear layer almost remains circular due to the fact that the primary vortex rings are not generated at the position. On the other hand, in the controlled jet, the azimuthal deformation becomes much intense, and rib structures can be clearly observed in the vortex ring ($\phi = 0.2\pi$) and the braid region ($\phi = \pi$). These structures derive from azimuthal instabilities amplified by the periodic vortex ring shedding and contribute to breakdown of the primary vortices and development of streamwise vortices further downstream [17]. Generally, the rib structures composed of counter-rotating pair are generated in a no-swirling jet. In contrast, in the swirling jet, the asymmetric ribs, which are anti-cyclonical with respect to the base flow rotation (A in the figure), are formed. This feature is in accordance with the results of Loiseleux and Chomaz [18] in single swirling jet.

Figure 15 shows instantaneous cross-sectional images and corresponding velocity fields for the uncontrolled and controlled jet with St_a = 1.0 at z/D_o = 2.0, where the primary vortex rings produced by the flap already break down as shown in Fig. 8. The velocity vectors are measured through the stereo-PIV technique and contours of second invariant of deformation tensor Q (< 0) is superimposed in the figure. In the uncontrolled jet, six rib structures, which coincide with the number of the swirler blades, can be observed. This implies that the amplification of azimuthal instabilities in a swirling jet is strongly dependent on geometry of swirler employed. On the other hand, in the controlled jet, it is found that the jet width is developed significantly and the number of streamwise vortices is increased to almost five times as that of the uncontrolled jet. Since the strength of these streamwise vortices is comparable with the primary vortex ring, it is anticipated that they contribute to the mixing enhancement in the downstream region.

4. Conclusions

In the present study, the large-scale vortical structures and associated mixing in the methane/air swirling coaxial jet are actively controlled by the outer shear layer excitation with the arrayed micro flap actuators. The influences of swirl intensity and flapping St_a on the control effect are investigated through stereo-PIV and PLIF techniques.

As a result, it is found that large-scale vortex rings can be shed perfectly in phase with the flapping motion in the outer swirling jet shear layer regardless of the swirl intensity tested. On the other hand, the vortical structures in the inner shear layer is strongly dependent on the swirl rate. In the coaxial swirling jet, the central jet is accelerated due to the pressure gradient generated by the swirl in the annular jet and it increases rapidly with increase in the swirl intensity. Therefore, at a high swirl rate (S = 0.4), the momentum flux ratio, $\rho_o U_o^2 / \rho_i U_i^2$, at the nozzle near-field is significantly reduced, so that the vortex formation in the inner shear layer is suppressed. Thus, it is effective for the swirling coaxial jet control to set initial momentum flux ratio, $\rho_o U_{m,o}^2 / \rho_i U_{m,i}^2$, relatively low by adjusting the ratio of nozzle diameters D_o/D_i.

At a low swirl rate (S = 0.2), relatively intense vortices are produced in the inner shear layer, and thus the mixing of central methane and annular air flows can be controlled. Since the central jet is also accelerated in this lower swirl condition, the inner vortices are weakened compared to the controlled no-swirling coaxial jet [7]. However, when $St_a \geqq 1.0$, the inner

vortices are shed continuously and pinch off the central jet. This promotes the transport and mixing of methane/air fluids, and thus the flammable mixture with small fluctuation can be formed in the early stage unlike the uncontrolled jet. In addition, the diameter of the vortices becomes small as St_a is increased, so that the transport range can be controlled by changing St_a.

5. Acknowledgements

The first author (YS) was supported by the Grant-in-Aid for JSPS Fellows (21COE, No. 19-52263) of MEXT of Japan.

6. References

[1] S. C. Crow and F. H. Champagne, Orderly structure in jet turbulence, *J. Fluid Mech*., 48, 547-591, 1971.
[2] K. B. M. Q. Zaman and A. K. M. F. Hussain, Vortex pairing in a circular jet under controlled excitation, *J. Fluid Mech*., 101, 449-491, 1980.
[3] R. B. Wicker and J. K. Eaton, Near field of a coaxial jet with and without axial excitation, *AIAA J*., 32, 542-546, 1994.
[4] J. Panda and D. K. McLaughlin, Experiments on the instabilities of a swirling jet, *Phys. Fluids*, 6, 263-276, 1994.
[5] F. Gallaire, S. Rott, J. M. Chomaz, Experimental study of a free and forced swirling jet, *Phys. Fluids*, 16-8, 2907-2917, 2004.
[6] S. V. Alekseenko, V. M. Dulin, Y. S. Kozorezov and D. M. Markovich, Effect of axisymmetric forcing on the structure of a swirling turbulent jet, *Int. J. Heat Fluid Flow*, 29, 1699-1715, 2008.
[7] N. Kurimoto, Y. Suzuki and N. Kasagi, Active control of coaxial jet mixing with arrayed micro actuators, *JSME J B* (*in Japanese*), 70, 1417-1424, 2004.
[8] H. Suzuki, N. Kasagi, Y. Suzuki, Active control of an axisymmetric jet with distributed electromagnetic flap actuators, *Exp. Fluids*, 36, 489-509, 2004.
[9] M. M. Ribeiro and J. H. Whitelaw, Coaxial jets with and without swirl, *J. Fluid Mech*., 96-4, 769-795, 1980.
[10] K. Nagae, Y. Saiki and N. Kasagi, Mechanism of vortex generation and its contribution to mixing enhancement in a controlled coaxial jet, In *Sixth International Symposium on Turbulence and Shear Flow Phenomena*, 2009.
[11] A. Melling, Tracer particles and seeding for particle image velocimetry, *Meas. Sci. Tech*., 8, 1406-1416, 1997.
[12] A. K. Prasad, Stereoscopic particle image velocimetry, *Exp. Fluids*, 29, 103-116.
[13] R. D. Kean and R. J. Adrian, Theory of cross-correlation analysis of PIV images, *J. App. Sci. Res*. 49, 191, 1992.
[14] F. H. Champagne and S. Kromat, Experiments on the formation of a recirculation zone in a swirling coaxial jets, *Exp. Fluids*, 29, 494-504, 2000.
[15] A. K. Gupta, D. J. Lilley and N. Syred, Swirl flows, Tunbridge Wells, UK: Abacus Press, 1984.
[16] R. J. Adrian, K. T. Christensen and Z. C. Liu, Analysis and interpretation of instantaneous turbulent velocity fields, *Exp. Fluids*, 29, 275-290, 2000.
[17] D. Liepmann and M. Gharib, The role of streamwise vorticity in the near-field entrainment of round jets, *J. Fluid Mech*., 245, 643-668, 1992.
[18] T. Loiseleux and J. M. Chomaz, Breaking of rotational symmetry in a swirling jet experiment, *Phys. Fluids*, 15, 511-523, 2003.